



1 **Different trends between extreme and median surface aerosol extinction**
2 **coefficients over China inferred from quality controlled visibility data**

3 Jing Li^{1,*}, Chengcai Li¹, Chunsheng Zhao¹

4 *Department of Atmospheric and Oceanic Sciences, School of Physics, Peking University,*
5 *Beijing, China, 100871*

7 **Abstract**

8
9 Although the temporal changes of aerosol properties have been widely investigated,
10 the majority focused on the averaged condition without much emphasis on the extremes.
11 However, the latter can be more important in terms of human health and climate change.
12 This study uses a previously validated, quality-controlled visibility dataset to investigate
13 the long-term trends of extreme surface aerosol extinction coefficient (AEC) over China,
14 and compare them with the median trends. Two methods are used to independently
15 evaluate the trends, which arrive at consistent results. The sign of extreme and median
16 trends are generally coherent, whereas their magnitudes show distinct spatial and
17 temporal differences. In the 1980s, an overall positive trend is found throughout China
18 with the extreme trend exceeding the mean trend, except for Northwest China and the
19 North China Plain. In the 1990s, AEC over Northeast and Northwest China starts to
20 decline while the rest of the country still exhibits an increase. The extreme trends
21 continue to dominate in the south while it yields to the mean trend in the north. After year



22 2000, the extreme trend becomes weaker than the mean trend overall in terms of both the
23 magnitude and significance level. The annual trend can be primarily attributed to winter
24 and fall trends. The results suggest that the decadal changes of pollution in China may be
25 governed by different mechanisms. Synoptic conditions that often result in extreme air
26 quality changes might dominate in the 1980s, whereas emission increase might be the
27 main factor for the 2000s.

28

29 1. Introduction

30

31 As a by-product of the rapid industrial and economic development, China has been
32 faced with a serious issue of air pollution. The variability and trends of China's air
33 quality or aerosol properties have become the focus of numerous past studies (*Jinhuan*
34 *and Liqun*, 2000; *Che et al.*, 2007; *Deng et al.*, 2008; *Streets et al.*, 2008; *Yoon et al.*,
35 2011; *Guo et al.*, 2011; *Zhang et al.*, 2015). While many of these works reached
36 important conclusions about the temporal evolution of China's pollution, the majority
37 only analyzed the arithmetic means (e.g., monthly or annual means of aerosol optical
38 depth), with little attention paid to the extreme values. However, it is often these extremes
39 that are responsible for many health and climate related aftermaths. Additionally,
40 considering that the distribution of aerosol optical properties, such as aerosol optical
41 depth (AOD) and extinction coefficients, are often highly right-skewed (*O'Neill et al.*,
42 2000; *Collaud Coen et al.*, 2013; *Yoon et al.*, 2016), analyzing the arithmetic mean tends



43 to discard the large portion of information in the long tails, thus biasing the result.
44 Moreover, as indicated by previous studies, extreme pollution events are often associated
45 with abnormal synoptic conditions (*Zheng et al.*, 2015; *Ye et al.*, 2016), whereas the mean
46 should be more prone to changes in the emission which increases pollution level overall.
47 Therefore, analyzing the changes in both the mean and extreme values would help
48 understand the factors influencing the variability of pollution.

49 For the few studies that did address temporal changes in the percentiles of aerosol
50 loading, usually either satellite or surface based remote sensing measurements are used,
51 such as Aerosol Optical Depth (AOD) retrievals from Moderate Resolution Imaging
52 Spectroradiometer (MODIS, *Sullivan et al.*, 2015) or the Aerosol Robotic Network
53 (AERONET, *Xia*, 2011; *Yoon et al.*, 2016). Nonetheless, remote sensing data is not ideal
54 for extreme analysis, mainly because it frequently misses heavy pollution conditions
55 likely associated with strict cloud screening (*Lin and Li*, 2016). As a result, the “real”
56 extremely high aerosol loadings cannot be well detected using remote sensing. On the
57 other hand, surface visibility observations that do not require cloud screening or other
58 retrieval assumptions, can serve as a suitable alternative for pollution related research.
59 After eliminating fog, rain or snow conditions, degradation of surface visibility can be
60 mainly attributed to aerosol extinction and are thus closely related to air quality (*Husar et*
61 *al.*, 2000). Moreover, since routine visibility observation started as early as 1970s for
62 many sites, these data can offer a much longer time series for trend analysis than remote
63 sensing products. Previously, *Li et al.* (2016) used a quality controlled visibility dataset to



64 study temporal changes of monthly mean surface aerosol extinction in China for the past
65 30 years and found that there are obvious shifts in the trends for different time periods.
66 However, it still remains to understand whether the extreme values change faster or
67 slower than the mean.

68 In this paper, we use the same dataset as in *Li et al.* (2016) to further investigate the
69 trends of extremely high (defined as the 95th percentile) surface aerosol extinction
70 coefficients and compare them with the median trends representing averaged condition.
71 Although a threshold visibility value is often used in previous studies to define extreme
72 events (e.g., *Fu et al.* 2013 define extreme pollution as visibility lower than 5 km
73 conditions), the same threshold does not apply to all sites since their reporting
74 conventions may be different. We thus believe a percentile criterion would be more
75 appropriate. In addition to estimating the linear trend of the 95th percentile value itself, we
76 also use a novel method proposed by *Franzke* (2013) based on quantile regression with
77 surrogate data testing for significance, who used this method to test for significant trends
78 in extreme temperatures. To our knowledge, this method has not been applied to aerosol
79 related research, and the independent application of two methods increases the robustness
80 of the results.

81 In section 2, we describe the data and method used in this study. The analysis results
82 are presented in section 3, followed by the conclusions and a brief discussion in section 4.

83

84 2. Data and Methods



85

86 **2.1 Visibility data**

87

88 Here we use the same visibility dataset as in *Li et al.* (2016). This hourly surface
89 visibility dataset is obtained from the National Centers for Environmental Information
90 (NCDC, <http://www1.ncdc.noaa.gov/pub/data/noaa/>) of the National Oceanic and
91 Atmospheric Administration (NOAA). The data selection criteria and quality control
92 procedure strictly follows those implemented by *Li et al.* (2016). Briefly, data before
93 1980 is not used because of different reporting standard (*Che et al.*, 2007; *Wu et al.*,
94 2012). Those after 2013 are also excluded because many sites have replaced human
95 observation with automatic visibility sensors. Then the eight quality assurance steps
96 proposed by *Li et al.* (2016) is applied to the dataset. A total of 272 sites are selected for
97 China, whose data have been manually inspected to show no observable jumps or spikes.

98 The visibility is further converted to Aerosol Extinction Coefficient (AEC) using the
99 Koschmieder formula (*Koschmieder*, 1926), and corrected for relative humidity effects
100 according to *Husar and Holloway* (1984) and *Che et al.* (2007). This AEC dataset has
101 also been validated against surface PM_{2.5} and PM₁₀ measurements. Please refer to *Li et al.*
102 (2016) for detailed description of the correction and validation processes.

103

104 **2.2 Trend analysis methods**

105



106 We define extremes as the 95th percentile of the visibility converted surface AEC. To
 107 estimate trend of the extremes, we use two independent methods. The first is to obtain an
 108 annual or seasonal time series of the 95th percentile of the extinction coefficients and then
 109 perform a *Sen's* slope (*Sen*, 1968) estimate of its linear trend. The *Sen's* slope b is
 110 calculated as

$$111 \quad b = \text{Median}\left(\frac{X_i - X_j}{i - j}\right) \forall j < i \quad (1)$$

112 where X_i and X_j are the i th and j th value in the time series respectively.

113 Then the Mann-Kendall statistical test (*Mann*, 1945; *Kendall*, 1975) is applied to test
 114 whether the trend is significant at 95% level. The test statistic is calculated as

$$115 \quad S = \sum_{i=1}^{n-1} \sum_{j=i+1}^n \text{sgn}(X_j - X_i) \quad (2)$$

116 Where n is the number of data points, and sgn is the sign function:

$$117 \quad \text{sgn}(X_j - X_i) = \begin{cases} +1 & \text{if } X_j > X_i \\ 0 & \text{if } X_j = X_i \\ -1 & \text{if } X_j < X_i \end{cases} \quad (3)$$

118 The variance of S is given by

$$119 \quad \text{Var}(S) = \frac{1}{18} n(n-1)(2n+5) \quad (4)$$

120 If the sample size $n > 30$, which is well satisfied in our case, the standard normal test
 121 statistic ZS is computed using:



$$ZS = \begin{cases} \frac{S-1}{\sqrt{\text{Var}(S)}} & \text{if } S > 0 \\ 0 & \text{if } S = 0 \\ \frac{S+1}{\sqrt{\text{Var}(S)}} & \text{if } S < 0 \end{cases} \quad (5)$$

According to the normal distribution table, the 5% significance level is satisfied if $|ZS| > 1.96$.

The second approach is quantile regression, which is a well established method used in many previous studies (Koenker and Hallock, 2001; Hannachi, 2006; Barbosa *et al.*, 2011; Donner *et al.*, 2012; Franzke, 2013) to estimate extreme trends of climate data.

For regular linear least square regression, the model can be expressed as

$$E[y | \mathbf{X}] = \beta \mathbf{X} + \varepsilon \quad (6)$$

where y is the response variable conditioned on \mathbf{X} , and the β 's satisfy the minimization of the summed error function

$$\text{err} = \min \sum_i \xi(y_i - \beta X_i) \quad (7)$$

where

$$\xi(u) = u^2 \quad (8)$$

For linear quantile regression, the response variable becomes the τ th ($\tau \in [0,1]$) quantile of y conditioned on \mathbf{X} ,

$$Q_\tau[y | \mathbf{X}] = \beta \mathbf{X} + \varepsilon \quad (9)$$

where the β s still satisfy equation (2), but equation (3) now becomes

$$\xi_\tau(u) = \begin{cases} u\tau & u \geq 0 \\ u(\tau-1) & u < 0 \end{cases} \quad (10)$$



140 Note that ξ_τ is symmetric when $\tau = 0.5$, rotated to the right when $\tau < 0.5$ and to the
141 left when $\tau > 0.5$. The quantile regression problem can be numerically solved by linear
142 programming (Koenker and Hallock, 2001). Here we use the R package “quantreg” to
143 solve for the regression coefficients of daily mean AEC. Trends for both the 95th and 50th
144 (median) percentiles are estimated and the trends are compared. To test for significance
145 of the quantile regression trends, we adopt the bootstrap approach proposed by Franzke
146 (2013), who used surrogate data generated with the same autocorrelation function and the
147 same probability density function as the original dataset. The detailed generation
148 procedure can be found in Schreiber and Schmitz (1996) and Franzke (2013). Here we
149 generate 1000 surrogate time series to represent the intrinsic variability of the AEC time
150 series.

151 In addition, we also calculate the trends for the median AEC (50th percentile) using
152 the above two methods, and compare them with the extreme trends. All trends are
153 normalized and expressed as percentage change per decade.

154 Figure S1 in the supplement shows an example of the trend analysis using these two
155 methods. In the following text, to save space we only present trends using quantile
156 regression, whereas the Sen’s slope results, which agree well with the former, are
157 presented in the supplement material.

158

159 3. Results

160



161 **3.1 Trend Maps**

162

163 We first examine the distribution and temporal changes of trends for all sites in
164 China. As indicated by *Li et al.* (2016), there are significant temporal shifts of the
165 magnitude and sign of monthly mean AEC trends for different decades. We thus also
166 respectively examine the extreme and median trends for three consecutive decades:
167 1980-1990, 1991-2000 and 2000-2013. The overall trends for the 1980 to 2013 period are
168 weakly positive for the majority of the sites (see Figure S2).

169 The three columns in Figure 1 show the distribution of extreme trend (upper row),
170 median trend (middle row) and their differences (extreme minus median, bottom row) for
171 the 272 sites for the three periods respectively. To avoid the confusion caused by positive
172 and negative signs of the trend, the difference here are calculated using the absolute value
173 of the extreme and median trends. Larger dots in black circles mean that the trends are
174 statistically significant at 95% level. Figure 1 is the results from quantile regression,
175 whereas the trends using *Sen's* slope is presented in Figure S3, which shows largely
176 consistent pattern. It is seen from Figure 1 that the sign of median and extreme trends
177 mostly agree throughout China. An extensive positive trend is observed all over China in
178 the 1980s. During the 1990s, many sites, especially those in north China, began to
179 experience a decreased AEC. After year 2000, the north China sites continue to show
180 decreasing trends whereas AEC over many south China sites started to rise again.

181 However, a detailed comparison between median and extreme trends reveals distinct



182 spatial and temporal differences. Focusing on the bottom three panels of Figure 1 (g-h), it
183 is clear that in the 1980s, the extreme trends exceed the median trend throughout China,
184 with some differences as large as 50% (northwestern sites). The number of sites showing
185 significant extreme trend (178) is also greater than those with significant median trend
186 (91). Note that the number of significant sites can be different between quantile
187 regression and *Sen's* slope results, because (1) quantile regression is applied to daily data
188 while *Sen's* slope uses annual or seasonal percentiles and (2) quantile regression uses
189 bootstrap method to test for significance while *Sen's* slope uses MK test. Nonetheless, the
190 spatial patterns of the two methods are consistent. In the 1990s, the distribution of the
191 trend differences switched to a north-south “dipole” pattern, with negative values in the
192 north and positive in the south in general, i.e., extreme trends are weaker than the median
193 trend in the north but stronger in the south, with a rough separation at 33°N marked by
194 the horizontal black line on Figure 1h. In the north, the sites showing significant extreme
195 trends also becomes fewer than those with significant median trends in the north. Even in
196 the south, the difference between the extreme and median trends is much smaller
197 compared to the 1980s, indicating a slowdown of the increase in the extreme values.
198 After year 2000, almost the entire China exhibits a “blue” pattern as opposed to the “red”
199 pattern in the 1980s. Except for a few sites in central south China, the majority exhibits a
200 weaker extreme trend than the mean trend. There are also fewer sites showing significant
201 trends in the extreme (52) than in the median (119). This feature is particularly strong for
202 northeast, northwest and south China. Although east and south China still show positive



203 AEC trends, this result suggest that in this decade, the extreme pollution conditions have
204 not increased as much as the mean or background pollution.

205 In short, the positive trends in the 1980s over China can be primarily attributed an
206 increase in the extremes. The 1990s experienced with a transition, with extreme trends
207 becoming weaker than the median trend in the north and only slightly stronger in the
208 south. Finally in the 2000s, the extreme trends largely yield to the median trends.

209

210 **3.2 Regional Trends**

211

212 To examine the spatial and temporal changes in more detail, we further divide the
213 country into six representative regions, marked by black rectangles on Figure 1b. Three
214 of these regions: the North China Plain (NCP), Yangtze River Delta (YRD), and Pearl
215 River Delta (PRD) are the major urban conglomerates in China. Since the change in the
216 extreme and median is essentially related to the shift of the distribution, we first evaluate
217 the regional AEC distributions for the three decades. Figure 2 plots these distributions by
218 region on logarithmic scale, as AEC is usually considered to follow a lognormal
219 distribution (*Collaud Coen et al.*, 2013). The dashed lines in Figure 2 indicate location of
220 the 95th percentile. For all regions, there is a rightward extension of the tail of the
221 distribution from 1990s to 1980s, implying an increase of the extremes, which is also
222 characterized by the rightward shift of the 95th percentile line. NCP, YRD and NW China
223 also show a rightward shift of the distribution peak. From 1990s to 2000s, although the



224 distribution peak shifts to the right for PRD, YRD, SW China and NE China, there is no
225 obvious shift in the tail for these four regions. For the other two regions, NCP and NW
226 China, there is a leftward shift in both the peak and the tail, but the shift of the peak is
227 stronger. Overall, we can roughly conclude that the 1980s' AEC trend is characterized by
228 a change of the extremes, while in the 2000s the median dominates the trend.

229 Consistent with *Li et al.* (2016), we also calculate trends successively for all periods
230 starting each year from 1980 to 2004 and ends in 2013 with 10-year increments. Figure 3
231 shows the temporal evolution of the quantile regression trend differences with x axis
232 indicating the trend calculation start year and y axis indicating the length of the time
233 series, with its counterpart using *Sen's* slope shown by Figure S4. To save space, only the
234 absolute differences between the extreme and median trends are presented in Figure 3,
235 while their respective values are shown in Figures S5 and S6 for quantile regression and
236 Figures S7 and S8 for *Sen's* slope. The time series and linear trends for each region are
237 presented in Figure S9. Because in Figure 3 the trends are calculated successively for
238 each period, it helps to examine the time node of the changes more precisely. For
239 example, although Figures 1 and 2 both indicate that the extremes increase more rapidly
240 in the 1980s, for YRD and PRD, the duration is short with the extreme trend exceeding
241 the median trend since around 1982, while for the rest four regions the change happened
242 around 1986 or later. YRD, PRD and NE China experienced a short period of stronger
243 extreme trend from ~1994 to 1996, whereas the other three regions show weaker extreme
244 trends. After 2002, SW and NW China display a slightly higher extreme trend, which is



245 different from the rest four regions. These features suggest that there can be minor
246 differences when the trends are examined for different time periods.

247 The seasonal time series of the difference between extreme and median quantile
248 regression trends are plotted in Figure 4, with a 4-year moving average to smooth out
249 small wrinkles (its counterpart using *Sen's* slope is shown in Figure S10). Note that
250 Figure 4 shows the evolution of the trend difference for every ten-year period from 1980
251 to 2004 (i.e., 1980-1989, 1981-1990,..., 2004-2013). An outstanding feature in Figure 4 is
252 that for all regions, the summer (JJA) trend difference (indicated by red curves) exhibit
253 quite different, or even reversed variability from the other three seasons and the annual
254 result. For NE, NW China and the PRD, spring (MAM) trends also have relatively larger
255 departure. In general, winter (DJF) and fall (SON) trends agree better with the annual
256 trend. Since these two seasons are dominated by anthropogenic aerosols such as sulfate,
257 nitrate, black and organic carbon throughout China (*Cao et al.*, 2007; *Wang et al.*, 2007;
258 *Wang et al.*, 2015), the results indicate that changes in anthropogenic aerosol loading are
259 primarily responsible for the observed extreme and median trends. In the spring many
260 regions are influenced by dust, and in the summer, the relative humidity effect may
261 significantly enhance aerosol extinction. Both are natural factors and should have minor
262 contribution to the annual trend according to Figure 4.

263

264 4. Conclusions and Discussion

265



266 While the trends of aerosol pollution in China have been studies extensively, it
267 remains to understand whether the extreme conditions have changed and whether their
268 changes are faster or slower than the mean. In this study, we use a quality controlled
269 visibility dataset to examine decadal trends of extreme values of surface aerosol
270 extinction coefficients. Quantile regression and *Sen's* slope estimates are jointly used to
271 estimate the trends to improve its robustness. Our analysis reveals that in general, the
272 extreme and median trends agree in terms of the sign, but they can differ significantly in
273 terms of the amplitude. During the 1980s, the extremes increased faster than the median
274 for most China except for a few north and northwest sites. The 1990s experienced a
275 transition with extreme trend becoming weaker than median trend in the north but still
276 slightly stronger in the south. Then in the 2000s, the majority of the country exhibited a
277 weaker extreme trend than the median trend. Seasonally, winter and fall trends are the
278 most consistent with annual trends, while the summer trend shows the largest departure
279 from the annual trend.

280 This study uses daily mean daytime AEC without accounting for its diurnal
281 variability. Nonetheless, visibility can still change considerably in the course of a day
282 (*Deng et al.*, 2011). To examine this effect we repeat the analysis using daily minimum
283 and daily maximum AEC respectively. Their counterparts of Figure 1 are shown in
284 Figures S11 and S12. A brief comparison indicates high resemblance of these two figures
285 to Figure 1 that uses daily mean data, albeit with some reasonable differences in the
286 amplitude.



287 The reason for the different behaviors between the extreme and median trends still
288 needs further investigation, and will be the topic of our future study. Some implication is
289 that in the 1980s and part of 1990s, synoptic conditions might be playing a major role in
290 modulating aerosol variability. For example, several extremely heavy pollution events are
291 believed to be linked to stagnant weather (*Tao et al.*, 2014; *Zheng et al.*, 2015). After mid
292 1990s, emission might become more dominate which tends to increase both the extreme
293 and the mean. But since it is a relatively uniform background change, the signal might be
294 more prominent in the mean condition. On the other hand, aerosol properties can also be
295 potentially influenced by decadal or interannual climate variability (*Chen and Wang*,
296 2015; *Wang and Chen*, 2016), whose footprint may be embedded in these extreme and
297 mean trends. However, the mechanism that they impact on the extremes and the mean
298 still need to be understood, and likely require a comprehensive study using both
299 observations and model simulations. This also requires the models to accurately simulate
300 the extreme events, which is a challenging task.

301 Admittedly, the visibility data is not ideal for aerosol-related studies, given its
302 various sources of uncertainties as discussed in *Li et al.* (2016). However, it is a currently
303 best compromise since there is lack of reliable long-term aerosol observation datasets.
304 Moreover, remote sensing produces are vulnerable to extreme pollution, making them
305 unsuitable for extreme trend studies. For example, as discussed in *Lin and Li* (2013),
306 MODIS frequently misses the heavy haze over north China likely due to cloud screening
307 algorithm. Sun photometers will also stop working when the sun is blocked by the heavy



308 pollution. This also suggests that current remote sensing instruments and retrieval
309 algorithms need to be improved to observe these extreme events.

310

311 **Acknowledgements**

312 We thank the NOAA NCDC database for providing the hourly visibility
313 measurements used for this study. The data is downloaded from the NCDC public ftp at
314 <http://www1.ncdc.noaa.gov/pub/data/noaa/>. This work is funded by National Science
315 Foundation of China Grants No. 41575018 and No. 41530423, and the 1000-Young
316 Talent program of China.

317

318 **References**

319

320 Barbosa, S. M. (2011), Testing for Deterministic Trends in Global Sea Surface

321 Temperature, *J. Climate*, 24, 2516–2522, doi:10.1175/2010JCLI3877.1.

322 Cao, J. J., et al. (2007), Spatial and seasonal distributions of carbonaceous aerosols over

323 China, *J. Geophys. Res.*, 112, D22S11, doi:10.1029/2006JD008205.

324 Che, H., X. Zhang, Y. Li, Z. Zhou, and J. J. Qu, (2007). Horizontal visibility trends in

325 China 1981–2005. *Geophys. Res. Lett.*, 34(24).

326 Chen, H. P., and H. J. Wang (2015), Haze days in North China and the associated

327 atmospheric circulations based on daily visibility data from 1960 to 2012. *J. Geophys.*

328 *Res. Atmos.*, 120(12), 5895-5909.



- 329 Collaud Coen, M., Andrews, E., Asmi, A., Baltensperger, U., Bukowiecki, N., Day, D.,
- 330 Fiebig, M., Fjaeraa, A. M., Flentje, H., Hyvärinen, A., Jefferson, A., Jennings, S. G.,
- 331 Kouvarakis, G., H. Lihavainen, C. Lund Myhre, W. C. Malm, N. Mihapopoulos,
- 332 J.V. Molenar, C. O'Dowd, J. A. Ogren, B. A. Schichtel, P. Sheridan, A. Virkkula, E.
- 333 Weingartner, R. Weller, P. and Laj, P. (2013), Aerosol decadal trends – Part 1: In-situ
- 334 optical measurements at GAW and IMPROVE stations, *Atmos. Chem. Phys.*, 13,
- 335 869-894, doi:10.5194/acp-13-869-2013.
- 336 Deng, J., T. Wang, Z. Jiang, M. Xie, R. Zhang, X. Huang, and J. Zhu (2011).
- 337 Characterization of visibility and its affecting factors over Nanjing, China. *Atmos.*
- 338 *Res.*, 101(3), 681-691.
- 339 Deng, X., X. Tie, D. Wu, X. Zhou, X. Bi, H. Tan, F. Li and C. Jiang (2008). Long-term
- 340 trend of visibility and its characterizations in the Pearl River Delta (PRD) region,
- 341 China. *Atmos. Environ.*, 42(7), 1424-1435.
- 342 Donner, R. V., R. Ehrcke, S. M. Barbosa, J. Wagner, J. F. Donges, and J. Kurths (2012),
- 343 Spatial patterns of linear and nonparametric long-term trends in Baltic sea-level
- 344 variability, *Nonlin. Processes Geophys.*, 19, 95–111, doi:10.5194/npg-19-95-2012.
- 345 Fu, C., Wu, J., Gao, Y., Zhao, D., and Han, Z. (2013). Consecutive extreme visibility
- 346 events in China during 1960–2009. *Atmos. Environ.*, 68, 1-7.
- 347 Franzke, C. (2013), A novel method to test for significant trends in extreme values in
- 348 serially dependent time series, *Geophys. Res. Lett.*, 40, 1391–1395,
- 349 doi:10.1002/grl.50301.



- 350 Guo, J. P., X. Y. Zhang, Y. R. Wu, Y. Zhaxi, H. Z. Che, B. La, W. Wang and X. W. Li,
351 (2011). Spatio-temporal variation trends of satellite-based aerosol optical depth in
352 China during 1980–2008. *Atmos. Environ.*, 45(37), 6802–6811.
- 353 Hannachi, A. (2006), Quantifying changes and their uncertainty in probability
354 distributions of climate variables using robust statistics, *Clim. Dyn.*, 27, 301–317,
355 doi:10.1007/s00382-006-0132-X.
- 356 Husar, R. B., and J. M. Holloway (1984), The properties and climate of atmospheric haze,
357 in *Hygroscopic Aerosols*, edited by L. H. Ruhnke and A. Deepak, pp. 129–170,
358 *Deepak Publ.*, Hampton, Va.
- 359 Husar, R. B., J. D. Husar, and L. Martin (2000). Distribution of continental surface
360 aerosol extinction based on visual range data. *Atmos. Environ.*, 34(29), 5067–5078.
- 361 Jinhuan, Q., and Liquan, Y. (2000). Variation characteristics of atmospheric aerosol
362 optical depths and visibility in North China during 1980–1994. *Atmos. Environ.*, 34(4),
363 603–609.
- 364 Kendall, M. G. (1975), Rank Correlation Methods, *Griffin*, London.
- 365 Koenker, R., and K. F. Hallock (2001), Quantile regression, *J. Economic Perspectives*, 15,
366 143–156.
- 367 Koschmieder, H. (1926). Theorie der horizontalen Sichtweite. *Beitsaegel Physik zur*
368 *Atmosphere* 12, 33–55.
- 369 Li, J., C. Li, C. Zhao, and T. Su (2016), Changes in surface aerosol extinction trends over
370 China during 1980–2013 inferred from quality-controlled visibility data, *Geophys. Res.*



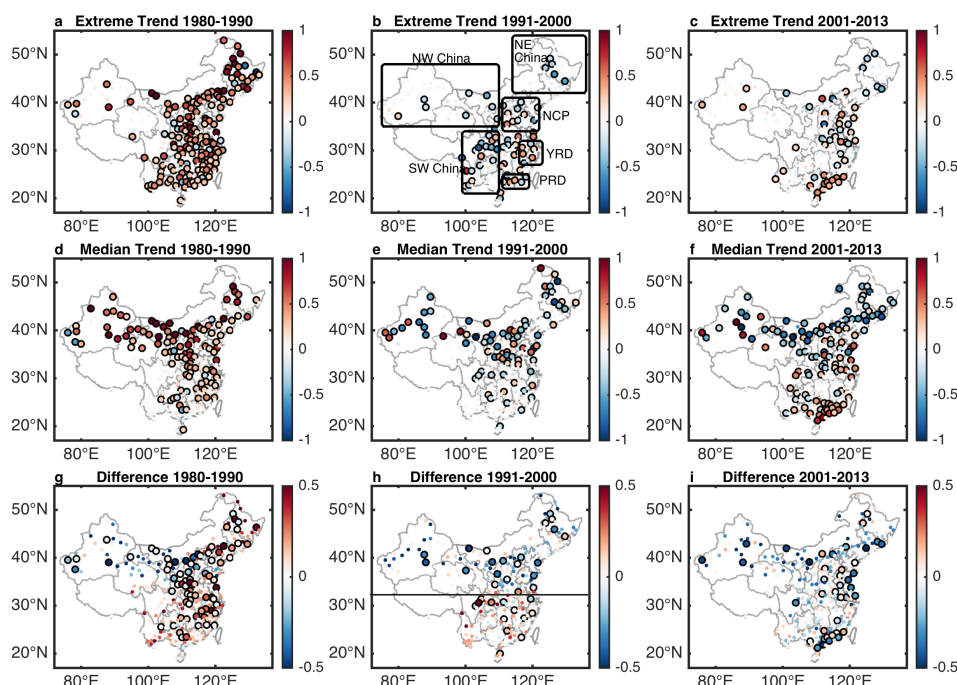
- 371 *Lett.*, 43, 8713–8719, doi:10.1002/2016GL070201.
- 372 Lin, J.-T., and J. Li (2016), Spatio-temporal variability of aerosols over East China
- 373 inferred by merged visibility-GEOS-Chem aerosol optical depth, *Atmos. Environ.*, 132,
- 374 111–122, doi:doi:10.1016/j.atmosenv.2016.02.037.
- 375 Mann H. B. (1945). Nonparametric tests against trend. *Econometrica* **13**: 245–259.
- 376 O’Neill, N. T., A. Ignatov, B. N. Holben, and T. F. Eck (2000). The lognormal
- 377 distribution as a reference for reporting aerosol optical depth statistics; Empirical tests
- 378 using multi-year, multi-site AERONET sunphotometer data. *Geophys. Res.*
- 379 *Lett.*, 27(20), 3333–3336.
- 380 Schreiber, T., and A. Schmitz (1996), Improved surrogate data for nonlinearity tests,
- 381 *Phys. Rev. Lett.*, 77, 635–638.
- 382 Sen, P. K. (1968), Estimates of the regression coefficient based on Kendall’s tau, *J. Am.*,
- 383 *Stat. Assoc.*, 63, 1379–1389.
- 384 Streets, D. G., C. Yu, Y. Wu, M. Chin, Z. Zhao, T. Hayasaka and G. Shi (2008). Aerosol
- 385 trends over China, 1980–2000. *Atmos. Res.*, 88(2), 174–182.
- 386 Sullivan, R. C., R. C. Levy and S. C. Pryor (2015). Spatiotemporal coherence of mean
- 387 and extreme aerosol particle events over eastern North America as observed from
- 388 satellite. *Atmos. Environ.*, 112, 126–135.
- 389 Tao, M., L. Chen, X. Xiong, M. Zhang, P. Ma, J. Tao and Z. Wang (2014). Formation
- 390 process of the widespread extreme haze pollution over northern China in January 2013:
- 391 Implications for regional air quality and climate. *Atmos. Environ.*, 98, 417–425.



- 392 Wang, G., K. Kawamura, X. Zhao, Q. Li, Z. Dai and H. Niu (2007). Identification,
393 abundance and seasonal variation of anthropogenic organic aerosols from a mega-city
394 in China. *Atmos. Environ.*, *41*(2), 407-416.
- 395 Wang, Q. Y., R.-J. Huang, J. J. Cao, X. X. Tie, H. Y. Ni, Y. Q. Zhou, Y. M. Han, T. F.
396 Hu, C. S. Zhu, T. Feng, N. Li, and J. D. Li (2015), Black carbon aerosol in winter
397 northeastern Qinghai–Tibetan Plateau, China: the source, mixing state and optical
398 property, *Atmos. Chem. Phys.*, *15*, 13059-13069, doi:10.5194/acp-15-13059-2015.
- 399 Wang, H. J. and H. P. Chen (2016), Understanding the recent trend of haze pollution in
400 eastern China: roles of climate change. *Atmos. Chem. Phys.*, *16*, 4205-4211.
- 401 Wu, J., C. Fu, L. Zhang and J. Tang, J. (2012). Trends of visibility on sunny days in
402 China in the recent 50 years. *Atmos. Environ.*, *55*, 339-346.
- 403 Xia, X. (2011). Variability of aerosol optical depth and Angstrom wavelength exponent
404 derived from AERONET observations in recent decades. *Environ. Res. Lett.*, *6*(4),
405 044011.
- 406 Ye, X., Y. Song, X. Cai and H. Zhang (2016). Study on the synoptic flow patterns and
407 boundary layer process of the severe haze events over the North China Plain in
408 January 2013. *Atmos. Environ.*, *124*, 129-145.
- 409 Yoon, J., W. von Hoyningen-Huene, M. Vountas and J. P. Burrows (2011), Analysis of
410 linear long-term trend of aerosol optical thickness derived from SeaWiFS using BAER
411 over Europe and South China, *Atmos. Chem. Phys.*, *11*, 12149-12167,
412 doi:10.5194/acp-11-12149-2011, 2011.



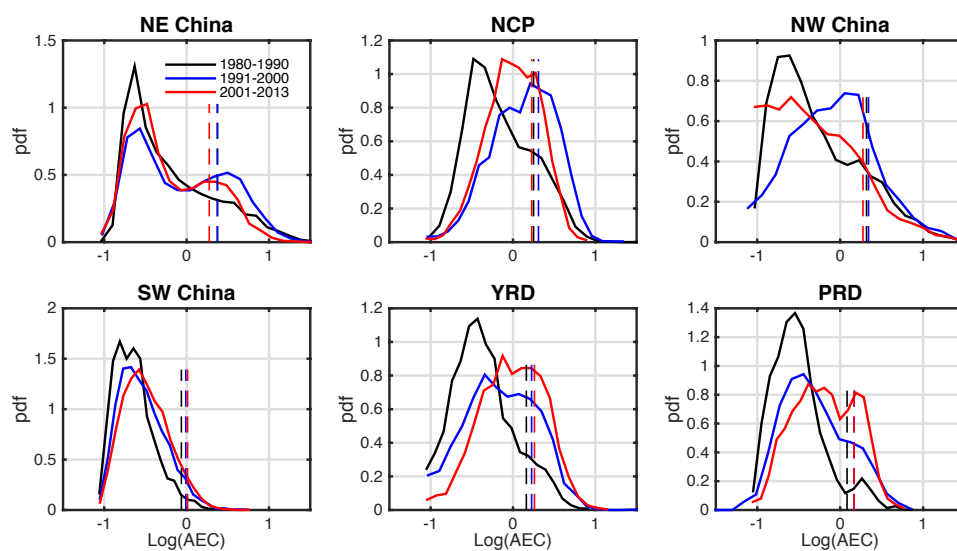
413 Yoon, J., A. Pozzer, D. Y. Chang, J. Lelieveld, J. Kim, M. Kim, Y. G. Lee, J.-H. Koo and
414 K. J. Moon (2016). Trend estimates of AERONET-observed and model-simulated
415 AOTs between 1993 and 2013. *Atmos. Environ.*, 125, 33-47.
416 Zhang, X., L. Wang, W. Wang, D. Cao, X. Wang and D. Ye (2015). Long-term trend and
417 spatiotemporal variations of haze over China by satellite observations from 1979 to
418 2013. *Atmos. Environ.*, 119, 362-373.
419 Zheng, G. J., F. K. Duan, H. Su, Y. L. Ma, Y. Cheng, B. Zheng, Q. Zhang, T. Huang, T.
420 Kimoto, D. Chang, U. Pöschl, Y. F. Cheng and K. B. He (2015), Exploring the severe
421 winter haze in Beijing: the impact of synoptic weather, regional transport and
422 heterogeneous reactions, *Atmos. Chem. Phys.*, 15, 2969-2983,
423 doi:10.5194/acp-15-2969-2015.
424



425

426 **Figure 1.** The first row: extreme trends estimate using quantile regression for the three
 427 decades, 1980-1990 (a), 1991-2000 (b), 2001-2013 (c); The second row: median trends
 428 estimated using quantile regression for the three decades; Bottom row: the difference
 429 between the values of the extreme trends and median trends, calculated as the extreme
 430 minus median.

431



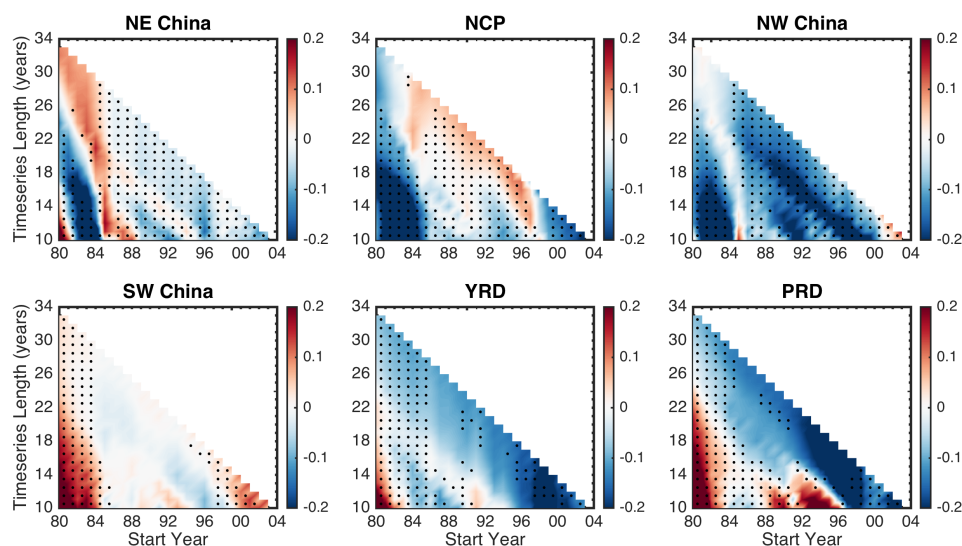
432

433 **Figure 2.** Probability distribution function (pdf) of AEC for the three decades over the six

434 representative regions marked on panel b of Figure 1. The AEC has been converted to

435 logarithmic scale.

436



437

438 **Figure 3.** Difference between extreme and median trends calculated using quantile

439 regression for the six representative regions marked on panel b of Figure 1. Trends are

440 between each year from 1980 to 2004 and the end of the record, with 10 minimum. The x

441 axis indicates the starting year, and the y axis indicates the length of the time series to

442 calculate the trend.

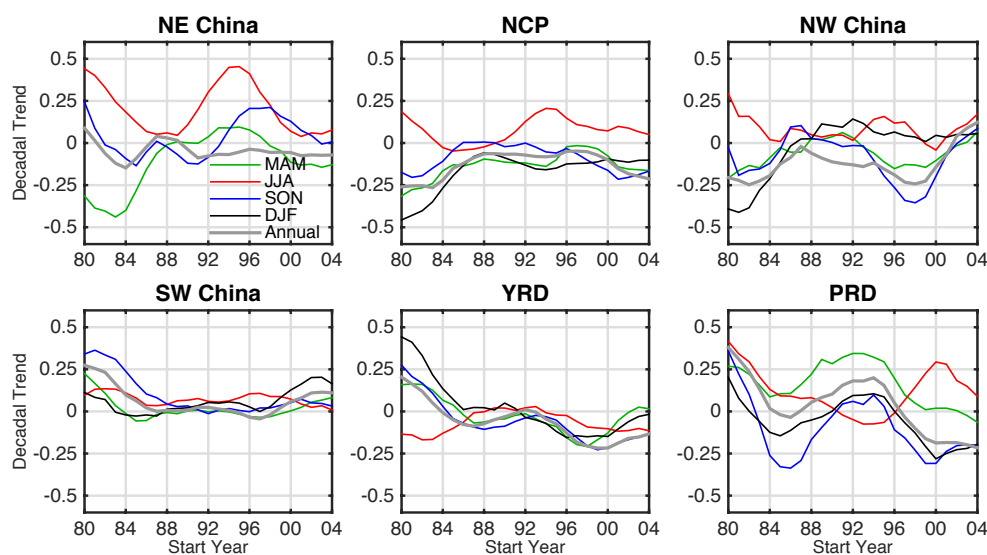


Figure 4. Seasonal time series of the difference between the extreme and median trends.

The trends are calculated for each 10 year period starting form 1980 to 2004 (x axis), i.e.,

the first point is the trend difference for the 1980 to 1989 period, the second from 1982 to

1990, etc.